## Introduction

Here we use the error metrics including the bias (b), RMSE (ε), correlation coefficient (ρ) and scatter index (SI) to investigate the sensitivity of the WW3 simulations to wind forcing (Sect. S1), the open boundary conditions (Sect. S2), current forcing (Sect. S3) and subgrid-scale reef parameterization S_{uo} (Sect. S4). The error metrics' definitions can be found, for example, in Liu et al. (2016, 2019). And following the method of Liu et al. (2021), error statistics of the significant wave height H_s gridded in 1°×1° bins are illustrated in Fig. S5. Details of the selected 28 buoys are provided in Table S1. Model results based on mesh version 2 are given in Sect. S6.

S1 Sensitivity to wind forcing
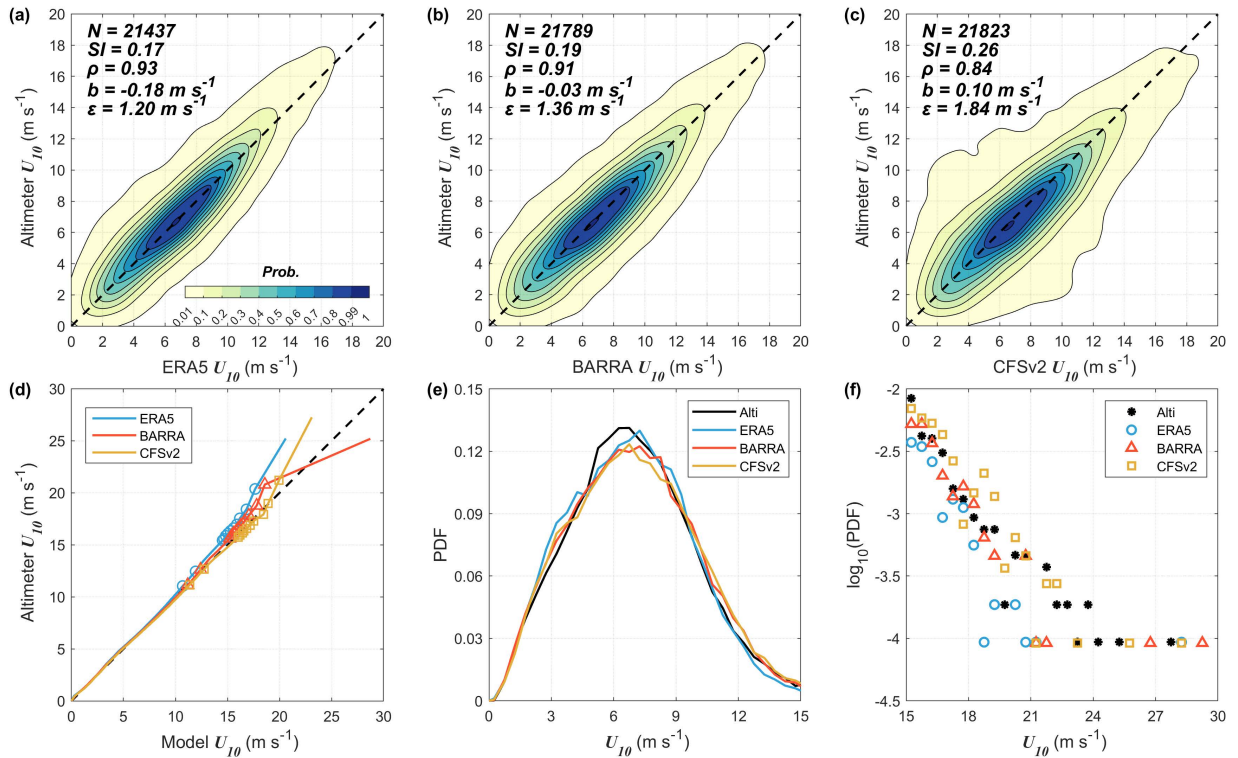
Figure S1: Comparison of wind forcings U_{10} between altimeters (ENVISAT, JASON-1, JASON-2 and CRYOSAT-2) and reanalysis (a) ERA5, (b) BARRA and (c) CFSv2 for 2011. (d) The percentile-percentile plot of U_{10} with markers highlighting the 90, 95, 99, 99.1, …, 99.9th percentiles. (e) Estimated probability density functions (PDFs) of U_{10} for $U_{10} < 15$ m s^{-1}. (f) Same as (e) but for the PDFs plotted on a logarithmic scale for $U_{10} > 15$ m s^{-1}.

A detailed intercomparison of the ERA5, CFSv2 and BARRA winds against the altimeter observations in 2011 is first conducted here to understand their relative performance along the Australian coast. Only winds over our WW3 model

domain are considered. Figure S1 shows that the ERA5 winds perform remarkably better than the other two reanalysis (Figs. S1a-c), with the highest correlation coefficient (ρ) of 0.93, and the lowest scatter index (SI) of 0.17 and RMSE (ε) of 1.20 m s^{-1}. The CFSv2 winds have the highest overall errors (e.g., $SI = 0.26$). Relative to the altimeter winds, the high-resolution BARRA is almost unbiased, but the ERA5 (CFSv2) is moderately biased low (high) with b of -0.18 (0.10) m s^{-1}. Inspection of the percentile-percentile plot (Figs. S1d-f) suggests all the three reanalysis winds perform well up to the 95th percentile of occurrence. In line with the findings of Liu et al. (2021) for global oceans, the ERA5 clearly underestimates extreme winds (e.g., $U_{10} \in [15,20]$ m s^{-1}), whereas the CFSv2 features good agreement with observations in this range. The BARRA lies in between the former two, much closer to the ERA5 percentiles. Nonetheless, it should be mentioned that altimeter winds might be questionable at very high winds (e.g., $U_{10} > 18$ m s^{-1}; Quilfen et al., 2011).
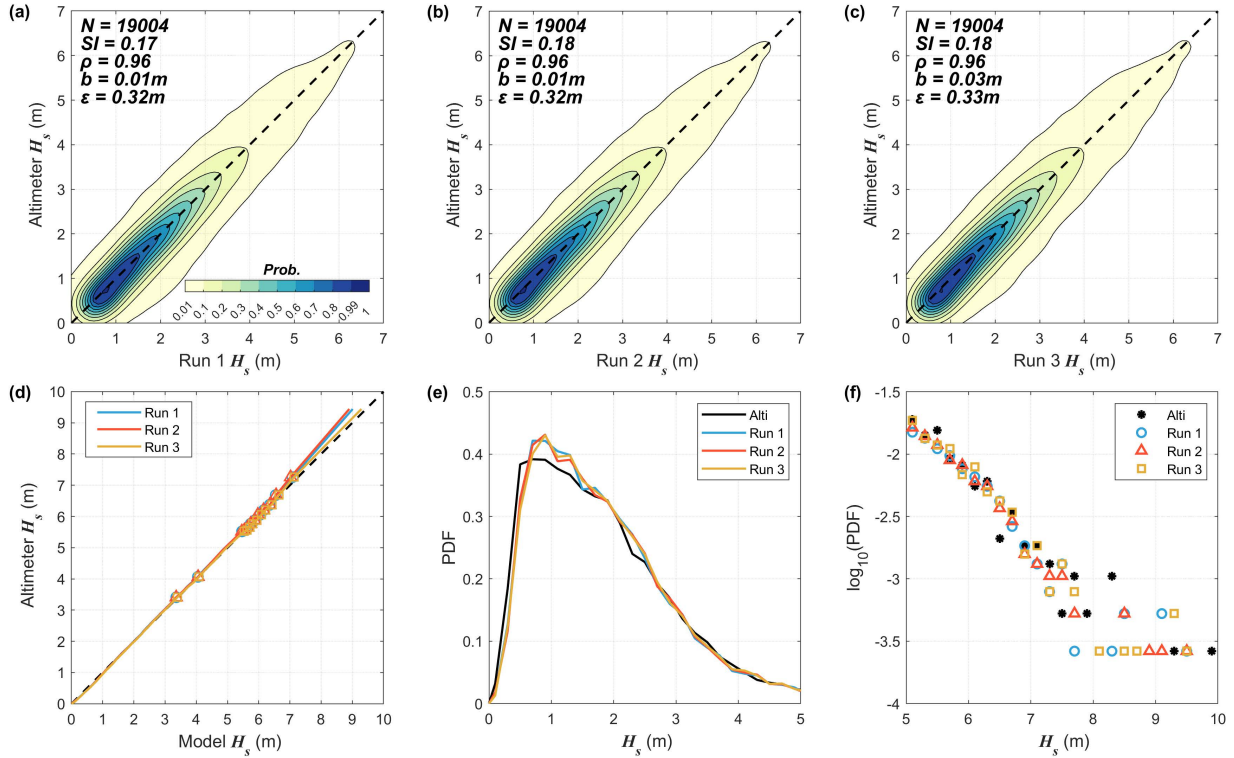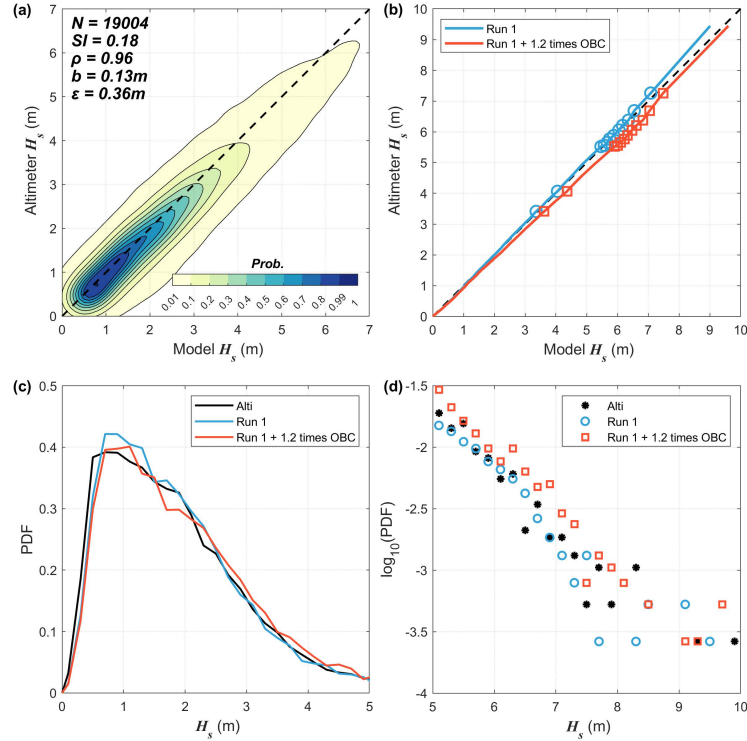

Figure S2: Comparison of the significant wave height H_s between altimeters (ENVISAT, JASON-1, JASON-2 and CRYOSAT-2) and WW3 outputs forced by the winds (a) ERA5 (CDFAC=1.08), (b) BARRA (CDFAC=1) and (c) CFSv2 (CDFAC=1) for 2011 (i.e., Runs 1-3 in Table 2). (d) The percentile-percentile plot of H_s with markers highlighting the 90, 95, 99, 99.1, …, 99.9th percentiles. (e) Estimated probability density functions (PDFs) of $H_s < 5$ m. (f) Same as (e) but for PDFs plotted on a logarithmic scale of $H_s > 5$ m.

The performance of the WW3-simulated wave heights from different runs forced by distinct reanalysis winds (i.e., Runs 1-3 in Table 2) is demonstrated in Fig. S2. Ocean currents and the source term S_{uo} were not considered in these runs. Following Liu et al. (2019, 2021), the tunable momentum flux parameter, CDFAC, for the ST6 source term package was set as 1.08 and

1 for the ERA5 and CFSv2 winds, respectively. We used CDFAC of 1 for BARRA as well. Nonetheless, as will be seen shortly, these moderate variations of the CDFAC make marginal differences in model results.

Despite the markedly different performance of the three winds as revealed in Fig. S1, the WW3 runs along the Australian coast forced by these winds yield a fairly consistent accuracy in wave height. As seen in Fig. S2, all the three runs feature a very high correlation of 0.96, a marginal bias (1-3 cm), a RMSE approximately 0.3 m and a relatively low SI of 0.17 (Figs. S2a-c). Even for high-percentile wave heights (e.g., $H_s > 5$ m), the three runs agree well with each other (Figs. S2d-f), as opposed to the apparent mismatch in extreme winds between the three reanalysis wind data (Figs. S1d-f). It was then quickly realized that owing to the relatively limited extent of our wave model domain (Fig. 1), the wave spectra at the open boundary points are likely more dominant than the wind forcing in regulating the model accuracy (Sect. S2).

Figure S3: (a) Comparison of the significant wave height H_s between altimeters (ENVISAT, JASON-1, JASON-2 and CRYOSAT-2) and WW3 outputs forced by the winds ERA5 (CDFAC=1.08) for 2011, but the open boundary conditions are adjusted to be 1.2 times those of Run 1. (b) The percentile-percentile plot of H_s with markers highlighting the 90, 95, 99, 99.1, …, 99.9th percentiles. (c) Estimated probability density functions (PDFs) of $H_s < 5$ m. (d) Same as (c) but for PDFs plotted on a logarithmic scale of $H_s > 5$ m.

S2 Sensitivity to open boundary conditions

To investigate the effect of open boundary conditions on model accuracy, a set of sensitive experiments was set up. The sensitive experiments are forced by the winds ERA5 (CDFAC = 1.08) for 2011 (i.e., Run 1 in Table 2), and the open

boundary condition (hereafter OBC) is the only variable (original OBC vs 1.2 times OBC). The original two-dimensional wave spectra $F(f, \theta)$ along open boundaries were sourced from the WW3-ST6 global wave hindcast of Liu et al. (2021). The 1.2 times OBC increases the bias of H_s from 1 cm in Run 1 (Fig. S2a) to 13 cm, and Fig. S3 shows the marked overestimation of H_s. Owing to the relatively limited extent of our wave model domain (Fig. 1), it could be corroborated that the wave spectra at open boundary points are more dominant than the wind forcing (Fig. S2) in regulating the model accuracy.

S3 Sensitivity to current forcing

Fig. S4 presents the statistical comparison between Runs 1, 4 and altimeters. Compared to the results of Run 1 (Fig. S2a), the inclusion of the ACCESS currents results in a very minor change in the overall model accuracy, with only a slight reduction of H_s (the bias changes from 0.7 cm in Run 1 to -0.3 cm in Run 4), largely due to the relative wind effect (e.g., Hersbach & Bidlot 2008).
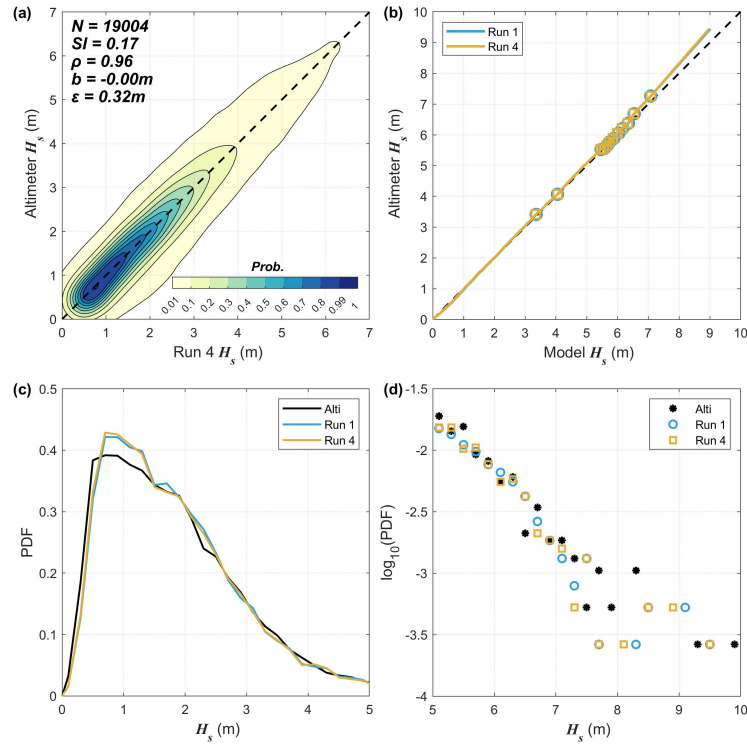
Figure S4: (a) Comparison of the significant wave height H_s between altimeters (ENVISAT, JASON-1, JASON-2 and CRYOSAT-2) and WW3 outputs forced by the winds ERA5 (CDFAC=1.08) and currents ACCESS for 2011 (i.e., Run 4 in Table 2). (b) The percentile-percentile plot of H_s with markers highlighting the 90, 95, 99, 99.1, …, 99.9th percentiles. (c) Estimated probability density functions (PDFs) of $H_s < 5$ m. (d) Same as (c) but for PDFs plotted on a logarithmic scale of $H_s > 5$ m.

S4 Sensitivity to subgrid scale reef parameterization S_{uo}

The spatial distribution of the absolute bias b and RMSE ε of H_s for the WW3 Runs 4, 5 relative to the altimeter wave
70   records is illustrated in Figs. S5a,b and Figs. S5c,d, respectively. The distribution characteristics of the absolute bias b are consistent with those of the normalized bias (see Figs. 7a, c). Except for the GBR, the model performs reasonably well with bias mostly ranging from -0.1 m to 0.1 m, and larger underestimation (-0.3 ~ -0.2 m) occurs offshore the state of New South Wales. The absolute RMSE is below 0.4 m for Southern coast of Australia and below 0.3 m for Northern coast of Australia.
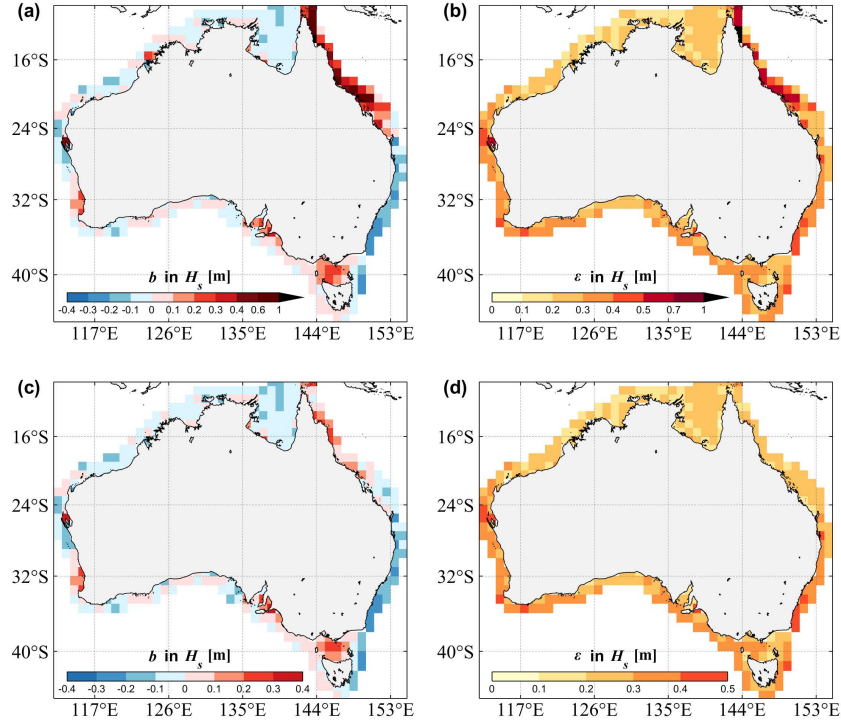
75   **Figure S5: Error statistics of the significant wave height H_s gridded in 1°×1° bins for the WW3 (a, b) Run 4 (without the S_{uo} approach) and (c, d) Run 5 (with S_{uo}) relative to the altimeter wave records: (a, c) the bias b, (b, d) normalized RMSE ε. The ERA5 winds and ACCESS currents were adopted to force these two runs.**

As discussed in Sect. 2.3, there are lots of individual reefs of the GBR could not be resolved by our unstructured mesh, so the dissipative effects of the GBR is totally neglected. Thus, the WW3 Run 4 seriously overestimates the H_s around the GBR,
80   with bias generally greater than 0.3 m and the maximum at 1.1 m. The RMSE in the GBR is also strikingly high with ε by and large above 0.5 m and the maximum at 1.2 m. The performance of the simulation with the reef parameterization S_{uo} is obviously improved (Figs. S5c,d vs Figs. S5a,b). It is seen that Run 5 (with S_{uo}) dramatically reduced the overestimation in the GBR, b is commonly below 0.2 m and RMSE is below 0.3 m.

S5 Buoys' information

85 **Table S1: List of buoys' information selected for validation. Buoys are identified by their wmo_id number (where assigned) or station name. Depth is the water depth at the buoy location used in the wave modeling and Domain is based on Australian administrative divisions.**

| wmo_id / site_name	LON/°	LAT/°	Depth/m	Domain
Albany 04	117.72	-35.20	62.42	WA
52121	141.68	-12.69	11.25	QLD
55035	153.63	-27.49	76.12	QLD
55040	136.62	-36.07	216.92	SA
55028	145.72	-16.73	15.10	QLD&GBR
Cottesloe	115.69	-31.98	15.46	WA
Esperance 04	121.90	-34.00	55.40	WA
Exmouth	114.09	-21.69	83.57	WA
55033	151.07	-23.31	19.55	QLD&GBR
55038	151.50	-23.89	17.75	QLD&GBR
55036	153.44	-27.96	18.14	QLD
55032	149.31	-21.27	8.97	QLD&GBR
Jurien Bay 02	114.91	-30.29	40.24	WA
55030	153.18	-26.57	32.67	QLD
Cape Naturaliste 02	114.76	-33.53	62.95	WA
Batemans Bay	150.34	-35.71	58.30	NSW
Byron Bay	153.70	-28.85	66.02	NSW
Coffs Harbour	153.27	-30.36	72.98	NSW
Crowdy Head	152.86	-31.82	77.39	NSW
Eden	150.19	-37.30	108.57	NSW
Port Kembla	151.03	-34.47	79.17	NSW
Sydney	151.41	-33.77	92.38	NSW
55027	153.28	-26.89	28.35	QLD
Cockburn	115.69	-32.11	10.50	WA
Rottnest Island 02	115.41	-32.09	63.71	WA
55026	145.03	-42.12	98.74	TAS
55029	147.06	-19.16	18.88	QLD&GBR
55037	153.58	-28.18	19.52	NSW

S6 Model results based on the higher-resoultion mesh (mesh version 2)

90   The spatial distribution of the normalized bias b_n and RMSE ε_n of H_s for the WW3 Runs 5, 7 relative to the altimeter wave records is illustrated in Figs. S6a,b and Figs. S6c,d, respectively. Figure S7 illustrates the impact of the reef parameterization S_{uo} on the simulated wave heights based on the high-resolution grid (i.e., Run 6,7 used mesh v2). When checking the spatial distributions of model errors in Run 5 (mesh version 1 with S_{uo}) and Run 7 (mesh version 2 with S_{uo}), we can observe that wave heights near the GBR is slightly reduced in Run 7 (Figs. S6e,f). The wave height bias of Run 7 is slightly decreased

95   (less than 10% for most of the GBR regions), indicating the dissipation, as represented by S_{uo}, is slightly stronger in Run 7 than in Run 5. Nonetheless, for these two km-scale simulations, Run 5 and Run 7 are still fairly close and both of these two runs show much better overall performance than Run 4 and Run 6 (Figs. S6, S7 and Fig. 7).
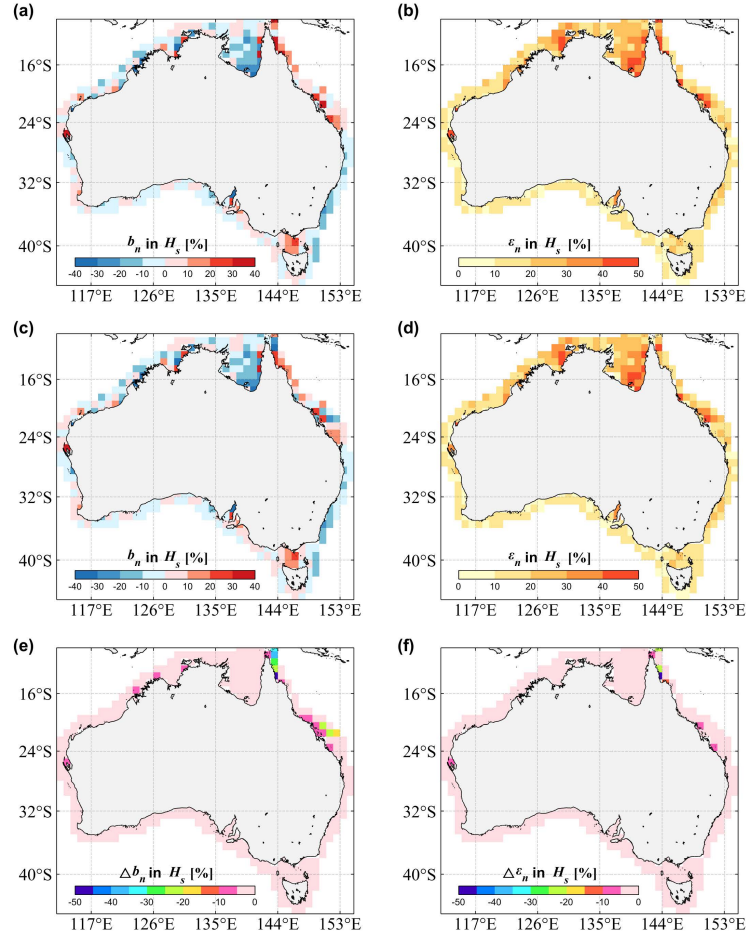
Figure S6: Error statistics of the significant wave height H_s gridded in 1°×1° bins for the WW3 for a two-month period (October – November 2011). (a, b) Run 5 (mesh v1 with S_{uo}) and (c, d) Run 7 (mesh v2 with S_{uo}) relative to the altimeter wave records: (a, c) the normalized bias b_n, (b, d) normalized RMSE ε_n. (e, f) Differences in H_s errors between the two WW3 runs: (e) $\Delta b_n = b_{n,7} - b_{n,5}$, (f) $\Delta \varepsilon_n = \varepsilon_{n,7} - \varepsilon_{n,5}$.

7
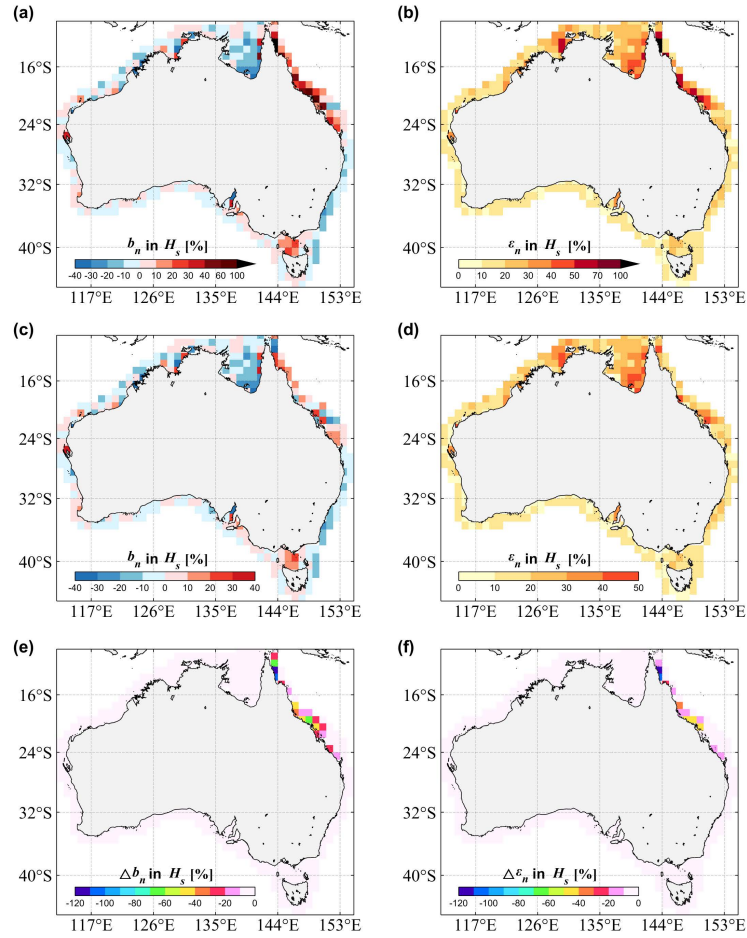
Figure S7: Error statistics of the significant wave height H_s gridded in $1°\times1°$ bins for the WW3 for a two-month period (October – November 2011). (a, b) Run 6 (mesh v2 without S_{uo}) and (c, d) Run 7 (mesh v2 with S_{uo}) relative to the altimeter wave records: (a, c) the normalized bias b_n, (b, d) normalized RMSE ε_n. (e, f) Differences in H_s errors between the two WW3 runs: (e) $\Delta b_n = b_{n,7} - b_{n,6}$, (f) $\Delta \varepsilon_n = \varepsilon_{n,7} - \varepsilon_{n,6}$.

Figure S8 shows directional wave spectra, 1D spectra and source terms from two different WW3 simulations (i.e., Run 5 used mesh v1 and Run 7 used mesh v2) at buoy 55032 at 1300 UTC 18 Oct 2011 (similar to Fig. 12). The balance of the source term at 55032 does change with increasing resolution. Moving from Run 5 to Run 7, S_{bf} (normalized by the wave spectrum) reduced slightly because of the increased water depth (9 m to 14 m). S_{uo} increases considerably because of changes in the transparency coefficients (i.e., α and β). But for the dominant wave direction (i.e., peak direction), S_{uo} in Run 7 is just about two times as large as S_{uo} in Run 5 (black square and black solid line in Fig. S8e).
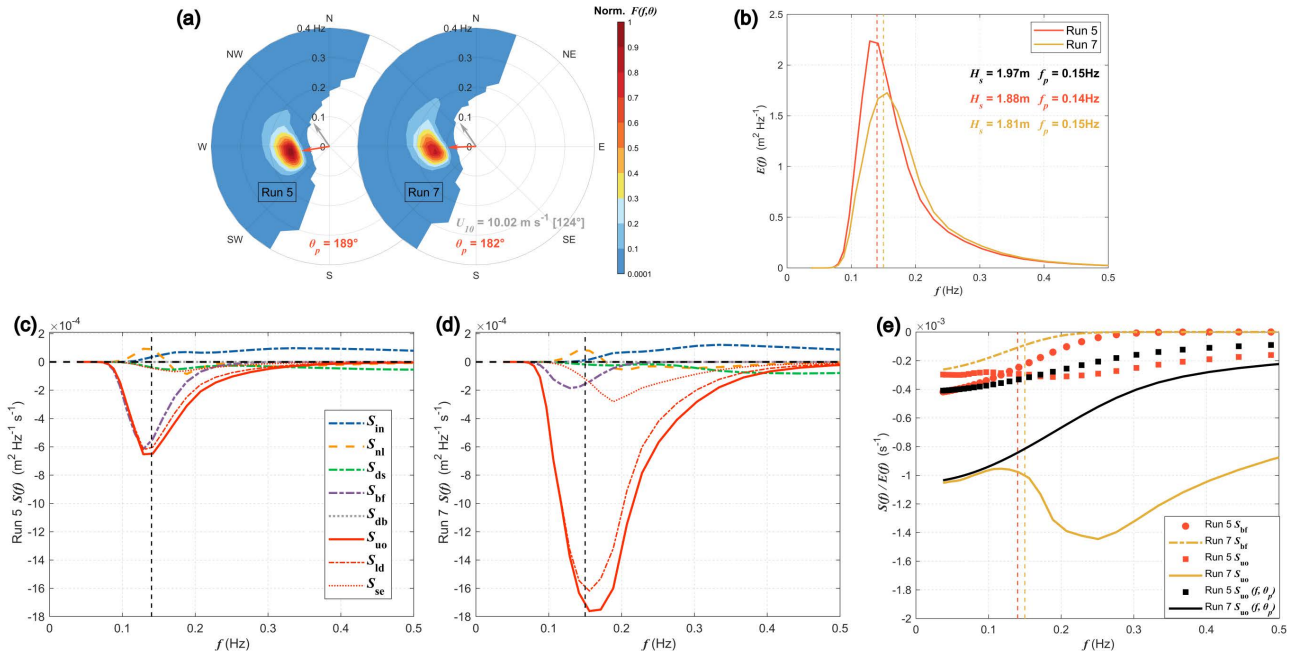
Figure S8: (a) Wave spectra $F(f,\theta)$ at buoy 55032 at 1300 UTC 18 Oct 2011 from Run 5 (used mesh v1, depth=8.97 m) and Run 7 (used mesh v2, depth=14.04 m), respectively. The grey and red arrows denote wind and peak wave directions. **(b)** The corresponding 1D wave spectra $E(f)$ with the respective wave height H_s and peak frequency f_p. Buoy observations are shown in black color. **(c, d)** The corresponding source terms for the spectra from Run 5 (used mesh v1) and Run 7 (used mesh v2), respectively. **(e)** The S_{bf} and S_{uo} normalized by the 1D wave spectra from Run 5 (used mesh v1) and Run 7 (used mesh v2), respectively. The black square and solid line represent the normalized S_{uo} at the peak wave direction. The vertical dashed lines in (b-e) represent locations of the peak frequency.

References

Hersbach, H., and Bidlot, J. R.: The relevance of ocean surface current in the ECMWF analysis and forecast system, in: Proc. ECMWF Workshop on Atmosphere-Ocean Interaction, vol. 6173, available at: https://www.ecmwf.int/sites/default/files/elibrary/2009/74791-relevance-ocean-surface-current-ecmwf-analysis-and-forecast-system_0.pdf , 2008.

Liu, Q., Babanin, A. V., Guan, C., Zieger, S., Sun, J., and Jia, Y.: Calibration and Validation of HY-2 Altimeter Wave Height, Journal of Atmospheric and Oceanic Technology, 33, 919–936, https://doi.org/10.1175/JTECH-D-15-0219.1, 2016.

Liu, Q., Rogers, W. E., Babanin, A. V., Young, I. R., Romero, L., Zieger, S., Qiao, F., and Guan, C.: Observation-Based Source Terms in the Third-Generation Wave Model WAVEWATCH III: Updates and Verification, Journal of Physical Oceanography, 49, 489–517, https://doi.org/10.1175/JPO-D-18-0137.1, 2019.

Liu, Q., Babanin, A. V., Rogers, W. E., Zieger, S., Young, I. R., Bidlot, J., Durrant, T., Ewans, K., Guan, C., Kirezci, C., et al.: Global Wave Hindcasts Using the Observation-Based Source Terms: Description and Validation, Journal of Advances in Modeling Earth Systems, 13, e2021MS002493, https://doi.org/10.1029/2021MS002493, 2021.

Quilfen, Y., Vandemark, D., Chapron, B., Feng, H., and Sienkiewicz, J.: Estimating Gale to Hurricane Force Winds Using the Satellite Altimeter, Journal of Atmospheric and Oceanic Technology, 28, 453–458, https://doi.org/10.1175/JTECH-D-10-05000.1, 2011.